Available online at www.sciencedirect.com
ScienceDirect
Trans. Nonferrous Met. Soc. China 26(2016) 2152−2161
Transactions of Nonferrous Metals Society of China
www.tnmsc.cn

Constitutive equation and processing map of equiatomic NiTi shape memory alloy under hot plastic deformation

Yan-qiu ZHANG[1], Shu-yong JIANG[1], Ya-nan ZHAO[1], Si-wei LIU[2]

1. School of Mechanical and Electrical Engineering, Harbin Engineering University, Harbin 150001, China;
2. Hubei Water Resources Research Institute, Wuhan 430070, China

Received 21 July 2015; accepted 11 April 2016

Abstract: In order to describe the deformation behavior and the hot workability of equiatomic NiTi shape memory alloy (SMA) during hot deformation, Arrhenius-type constitutive equation and hot processing map of the alloy were developed by hot compression tests at temperatures ranging from 500 to 1100 ℃ and strain rates ranging from 0.0005 to 0.5 s^{-1}. The results show that the instability region of the hot processing map increases with the increase of deformation extent. The instability occurs in the low and high temperature regions. The instability region presents the adiabatic shear bands at low temperatures, but it exhibits the abnormal growth of the grains at high temperatures. Consequently, it is necessary to avoid processing the equiatomic NiTi SMA in these regions. It is preferable to process the NiTi SMA at the temperatures ranging from 750 to 900 ℃.

Key words: NiTi alloy; shape memory alloy; hot plastic deformation; constitutive equation; hot processing map

1 Introduction

NiTi shape memory alloy (SMA) is a promising candidate for biomedical, control engineering and aerospace applications due to its excellent shape memory effect, superelasticity, corrosion resistance and mechanical properties [1−4]. Because of poor plasticity at room temperature, most high-quality products made from NiTi SMA should be subjected to hot deformation. It is very critical to reasonably control the process parameters in the case of hot deformation, so that high-quality products of NiTi SMAs are able to be obtained. Therefore, it is increasingly important to investigate the hot workability of NiTi SMA.

Over the recent decades, the concern for NiTi SMAs has been focusing on the thermo-mechanical processing, such as ausforming, marforming, severe plastic deformation and cold working followed by heat treatment [5−8]. Only a few literatures which involve hot deformation of NiTi SMAs can be found. In this regard, JIANG et al [9] investigated the hot deformation behavior of Ni−49.1%Ti (mole fraction) alloy and established the corresponding constitutive equation by hot compression tests. YEOM et al [10] optimized the hot forging process of Ni−49.6%Ti alloy by combining hot processing map with finite element method and obtained a sound NiTi billet without forging defects. SHAMSOLHODAEI et al [11] examined the constitutive behavior of Ni−49.9%Ti alloy through modified Zerillie−Armstrong and Arrhenius type models. MORAKABATI et al [12] developed the processing map of Ni−50.2%Ti alloy and determined the process parameters of NiTi alloy according to processing map.

However, all the above investigations are concerned with the near-equiatomic NiTi SMAs, which are either Ni-rich NiTi alloys or Ti-rich NiTi alloys. So far, few literatures which deal with constitutive equation and hot workability of the equiatomic NiTi SMA (Ti−50%Ni) have been found. Therefore, in the present study, the constitutive equation of hot deformation for the equiatomic NiTi SMA was investigated according to the compression tests, and the corresponding hot workability was studied on the basis of the hot processing map, which lays the foundations for obtaining the appropriate process parameters during hot deformation of equiatomic NiTi SMA.

Foundation item: Projects (51305091, 51305092, 51475101) supported by the National Natural Science Foundation of China; Project (20132304120025) supported by the Specialized Research Fund for the Doctoral Program of Higher Education, China
Corresponding author: Shu-yong JIANG; Tel: +86-13936266338; E-mail: jiangshy@sina.com
DOI: 10.1016/S1003-6326(16)64283-8

2 Experimental

The equiatomic NiTi SMA bar, which possessed nominal composition of Ni−50%Ti (mole fraction), was prepared by vacuum induction melting and subsequent hot rolling at 850 ℃. Based on differential scanning calorimetry (DSC), the phase transformation temperatures of the NiTi alloy were determined as M_s=33.6 ℃, M_f=10.8 ℃, A_s=44.4 ℃ and A_f=70.7 ℃. In order to obtain homogenous martensite structure, the NiTi alloy bar was held at 850 ℃ for 2 h and then quenched into the ice water. All the NiTi specimens used for experimental analysis were taken from the NiTi bar subjected to heat treatment along the longitudinal direction. The NiTi specimens for metallographic observation were etched in a solution with the composition of V(HF):V(HNO_3):V(H_2O)=1:2:5, and subsequently characterized by an OLYMPUS311 optical microscope. The NiTi specimens for TEM observation were thinned by twin-jet polishing in an electrolyte consisting of 34% $CH_3(CH_2)_3OH$, 6% $HClO_4$ and 60% CH_3OH by volume fraction. Subsequently, the NiTi specimens were characterized by TEM using an FEI TECNAI G2 F30 microscope. Figure 1 illustrates the microstructures of the NiTi bar subjected to heat treatment, where the equiaxed grains and the twin substructures can be observed. Twenty NiTi samples with the diameter of 4 mm and the height of 6 mm were used for compression tests. The tests were carried out on a INSTRON−5500R universal material testing machine. The samples were compressed by the deformation degree of 70% at the temperatures ranging from 500 to 1100 ℃ and the strain rates ranging from 0.0005 to 0.5 s^{-1}.

3 Results and discussion

3.1 Deformation behavior

Figure 2 illustrates the true stress–strain curves of the equiatomic NiTi SMA under compression at various temperatures and strain rates. It can be concluded that the true stress–strain curves exhibit the following characteristics. In the initial stage of the deformation, the true stress increases rapidly with the increase of the true stain. However, when the strain amounts to a certain value, the stress varies very slowly. Some of the curves decrease continuously, while others increase with the increase of the true strain and are followed by a period of decrease. The phenomenon is attributed to the competition between work hardening and dynamic softening of NiTi SMA. In the case of a constant deformation temperature, the true stress increases with the increase of the strain rate, which indicates that the equiatomic NiTi SMA is sensitive to the strain rate. Furthermore, the sensitivity at high temperatures is higher than that at low temperatures. In the case of a constant strain rate, the true stress decreases with the increase of the deformation temperature.

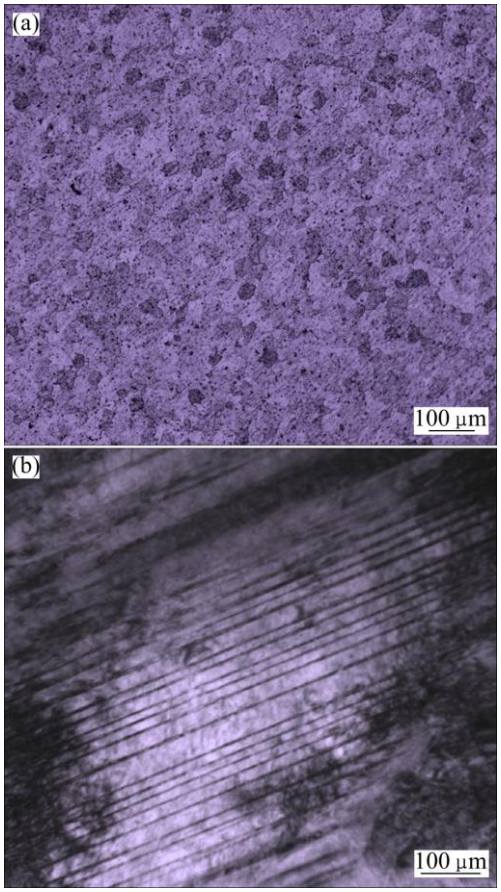

Fig. 1 Optical micrograph (a) and TEM image (b) of equiatomic NiTi SMA subjected to heat treatment

3.2 Constitutive equation

According to the true stress−strain curves of NiTi SMA at elevated temperature, the constitutive equation of NiTi SMA is established on the basis of the Arrhenius type equation [13,14]:

$$\dot{\varepsilon} = A[\sinh(\alpha\sigma)]^n \exp\left(-\frac{Q}{RT}\right) \quad (1)$$

where $\dot{\varepsilon}$ is the strain rate, σ is the flow stress which is taken as the peak stress in the present study, R is the mole gas constant (8.314 J/(mol·K)), T is the thermodynamic temperature, Q is the activation energy, and α, A and n are the material constants.

In order to further obtain the aforementioned material constants on the basis of the experimental data, it is convenient to simplify Eq. (1) mathematically [9].

When the low stress level leads to $\alpha\sigma \leq 0.8$, $\sinh(\alpha\sigma)=\alpha\sigma$ is approximately satisfied. As a consequence, Eq. (1) can be simplified as

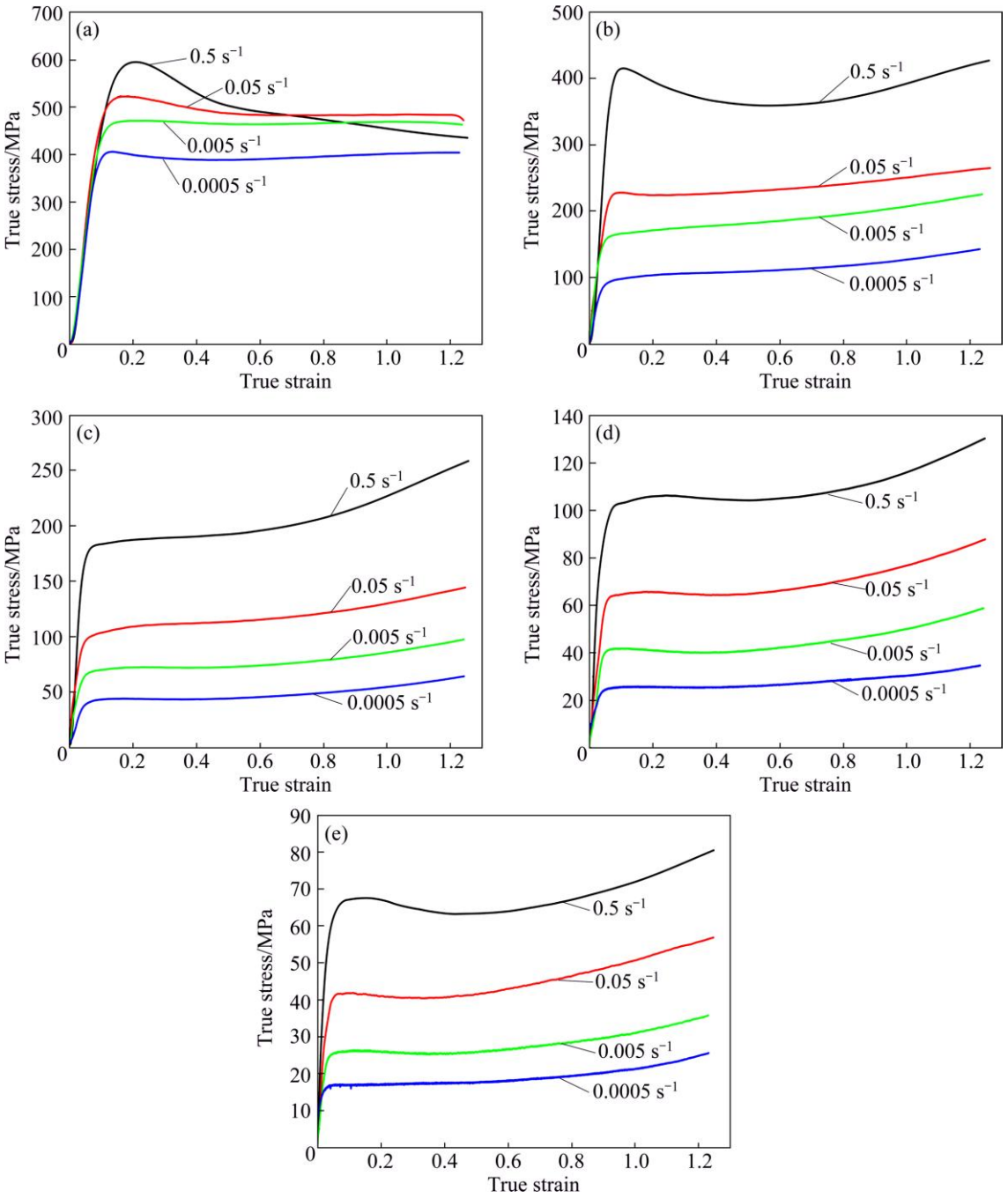

Fig. 2 True stress−strain curves of heat-treated equiatomic NiTi SMA under hot compression at various temperatures: (a) 500 ℃; (b) 650 ℃; (c) 800 ℃; (d) 950 ℃; (e) 1100 ℃

$$\dot{\varepsilon} = A(\alpha\sigma)^n \exp\left(\frac{-Q}{RT}\right) \quad (2)$$

Making $A_1=A\alpha^n$, Eq. (2) can be reduced to

$$\dot{\varepsilon} = A_1\sigma^n \exp\left(\frac{-Q}{RT}\right) \quad (3)$$

When the high stress level leads to $\alpha\sigma\geq1.6$, $\sinh(\alpha\sigma)=0.5\exp(\alpha\sigma)$ is approximately satisfied. As a result, Eq. (1) can be approximately expressed as

$$\dot{\varepsilon} = A/2^n[\exp(\alpha\sigma)]^n \exp\left(\frac{-Q}{RT}\right) \quad (4)$$

Having $A_2=A/2^n$ and $\beta=n\alpha$, Eq. (4) can be reduced to

$$\dot{\varepsilon} = A_2 \exp(\beta\sigma)\exp\left(\frac{-Q}{RT}\right) \quad (5)$$

The values of A, n, α and Q can be determined according to the experimental data in Fig. 2. Consequently, the constitutive equation of the equiatomic

NiTi SMA can be established.

To obtain the value of n, taking natural logarithm of both sides of Eq. (3) results in Eq. (6):

$$\ln\dot{\varepsilon} = \ln A_1 + n\ln\sigma - \frac{Q}{RT} \tag{6}$$

It can be seen from Eq. (6) that n is the linear proportion factor of $\ln\dot{\varepsilon}$ versus $\ln\sigma$ and thus can be determined via the linear fitting method in Fig. 3(a). The value of n is taken as the average value of the slopes of the fitted lines at various temperatures and thus is determined as 7.5434.

Similarly, to obtain the value of α, taking natural logarithm of both sides of Eq. (5) results in

$$\ln\dot{\varepsilon} = \ln A_2 + \beta\sigma - \frac{Q}{RT} \tag{7}$$

Equation (7) indicates that the value of β is the linear proportion factor of $\ln\dot{\varepsilon}$ versus σ and hence can be obtained by linear fitting method in Fig. 3(b). The value of β is calculated as the average value of the slopes of the fitted lines at various temperatures and thus is determined as 0.06465 MPa^{-1}. As a consequence, the value of α can be obtained by combining the values of n

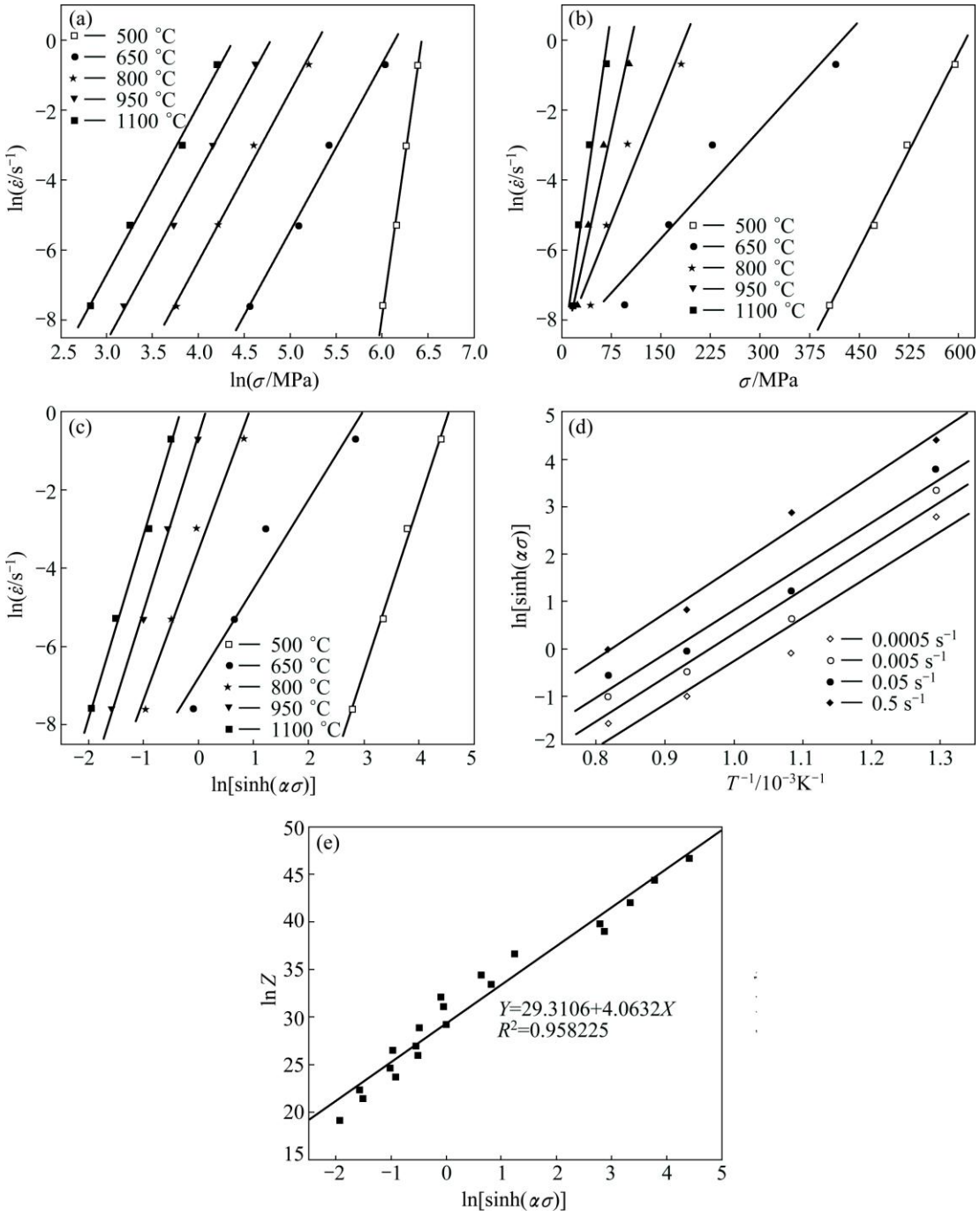

Fig. 3 Relationships among peak stress, strain rate, temperature and parameter Z: (a) $\ln\dot{\varepsilon}$ vs $\ln\sigma$; (b) $\ln\dot{\varepsilon}$ vs σ; (c) $\ln\dot{\varepsilon}$ vs $\ln[\sin(\alpha\sigma)]$; (d) $\ln[\sin(\alpha\sigma)]$ vs T^{-1}; (e) $\ln Z$ vs $\ln[\sinh(\alpha\sigma)]$

and β, namely $\alpha=\beta/n=8.57\times10^{-3}$ MPa^{-1}.

Because the above value of n is obtained at low stress level, it is necessary to optimize it so that it can be used under any conditions. Since Eq. (1) can be satisfied at any stress levels, the optimized value of n can be obtained by substituting the calculated value of α into Eq. (1).

A constant T leads to a constant Q. Therefore, taking natural logarithm of both sides of Eq. (1) results in

$$\ln\dot{\varepsilon}=\ln A+n\ln[\sinh(\alpha\sigma)]-\frac{Q}{RT} \tag{8}$$

Equation (8) indicates that the value of n is the linear proportion factor of $\ln\dot{\varepsilon}$ versus $\ln[\sinh(\alpha\sigma)]$ and thus can be determined via linear fitting method in Fig. 3(c). Then, the optimized value of n can be obtained by calculating the average value of the slopes of the fitted lines at various temperatures and thus is determined as 3.9339.

In the case of a constant strain rate $\dot{\varepsilon}$, taking natural logarithm of both sides of Eq. (1) results in Eq. (9),

$$\ln\dot{\varepsilon}-\ln A+\frac{Q}{RT}=n\ln[\sinh(\alpha\sigma)] \tag{9}$$

which can be rearranged to obtain the following form:

$$\ln[\sinh(\alpha\sigma)]=\frac{Q}{nR}\cdot\frac{1}{T}+\frac{\ln\dot{\varepsilon}-\ln A}{n}=\frac{Q}{nR}\cdot\frac{1}{T}+C_1 \tag{10}$$

where $C_1=(\ln\dot{\varepsilon}-\ln A)/n$, which is a constant in the case of a constant $\dot{\varepsilon}$, differentiating T^{-1} of both sides of Eq. (10) gives

$$Q=nR\left(\frac{\partial\ln[\sinh(\alpha\sigma)]}{\partial T^{-1}}\right)_{\dot{\varepsilon}} \tag{11}$$

where $\left(\frac{\partial\ln[\sinh(\alpha\sigma)]}{\partial T^{-1}}\right)_{\dot{\varepsilon}}$ is obtained by calculating the average value of the slopes of the fitted lines at various strain rates, as shown in Fig. 3(d). By substituting the values of the optimized n, R and $\left(\frac{\partial\ln[\sinh(\alpha\sigma)]}{\partial T^{-1}}\right)_{\dot{\varepsilon}}$ into Eq. (11), the value of Q is then determined as 3.0441×10^5 J/mol.

In general, the Zener–Hollomon parameter Z can be used to describe the comprehensive influence of the strain rate and the temperature on the flow stress of the metal materials during hot deformation [15].

$$Z=\dot{\varepsilon}\cdot\exp\left(\frac{Q}{RT}\right) \tag{12}$$

Combining Eq. (12) with Eq. (1) gives

$$Z=A[\sinh(\alpha\sigma)]^n \tag{13}$$

Taking natural logarithm of both sides of Eq. (13) gives

$$\ln Z=\ln A+n\ln[\sinh(\alpha\sigma)] \tag{14}$$

According to Eq. (14), ln A is just the intercept of the fitted line of ln Z versus $\ln[\sinh(\alpha\sigma)]$ on ln Z coordinate axis, as shown in Fig. 3(e), so that the value of A is further calculated as 5.3633×10^{12}.

By substituting the values of A, α, n and Q into Eq. (1), the constitutive equation of equiatomic NiTi SMA can be expressed as

$$\dot{\varepsilon}=5.3633\times10^{12}[\sinh(8.57\times10^{-3}\sigma)]^{3.9339}\times\exp\left(\frac{-3.0441\times10^5}{RT}\right) \tag{15}$$

Substituting Eq. (15) into Eq. (12) gives

$$Z=\dot{\varepsilon}\cdot\exp\left(\frac{Q}{RT}\right)=5.3633\times10^{12}[\sinh(8.57\times10^{-3}\sigma)]^{3.9339} \tag{16}$$

According to Eq. (13), the following equation can be obtained:

$$\sinh(\alpha\sigma)=(Z/A)^{1/n} \tag{17}$$

Based on the definition of hyperbolic sine, $\sinh(\alpha\sigma)$ can be expressed as

$$\sinh(\alpha\sigma)=\frac{\exp(\alpha\sigma)-\exp(-\alpha\sigma)}{2}=\frac{[\exp(\alpha\sigma)]^2-1}{2\exp(\alpha\sigma)} \tag{18}$$

Therefore, Eq. (17) can be further expressed as follows:

$$\sigma=\frac{1}{\alpha}\ln\left[\left(\frac{Z}{A}\right)^{1/n}+\sqrt{\left(\frac{Z}{A}\right)^{2/n}+1}\right] \tag{19}$$

In terms of the Zener–Hollomon parameter Z, the constitutive equation of equiatomic NiTi SMA is expressed as

$$\sigma=(1/\alpha)\ln\{(Z/A)^{1/n}+[(Z/A)^{2/n}+1]^{1/2}\}=116.686\ln\{[Z/(5.3633\times10^{12})]^{1/3.9339}+\{[Z/(5.3633\times10^{12})]^{2/3.9339}+1\}^{1/2}\} \tag{20}$$

Compared with the equation developed for a Ni-rich NiTi alloy, as shown in our early published paper [9], the constitutive equation obtained in this work is established for an equiatomic NiTi alloy. Furthermore, the value of the stress exponent n obtained in the present equation is smaller than the one in Ref. (9) and the activation energy Q is greater than the one in Ref. (9), which indicates that the composition of the alloy has a significant influence on the parameters of the constitutive equation.

3.3 Hot processing map

3.3.1 Fundamentals and methods of hot processing map

In terms of dynamic material model (DMM), hot processing maps are established on the basis of the true

stress−strain data, which are obtained in the hot compression tests. According to DMM, the power dissipated during plastic deformation of the materials can be described as [16]

$$P=\sigma\dot{\varepsilon}=G+J=\int_0^{\dot{\varepsilon}}\sigma \mathrm{d}\dot{\varepsilon}+\int_0^{\sigma}\dot{\varepsilon}\mathrm{d}\sigma \tag{21}$$

where G is the dissipated content, which represents the power dissipated during plastic deformation of the materials; J is the dissipated co-content, which represents the power dissipated during microstructure transformation of the materials.

For the given strain ε and temperature T, there exists the following dynamic relationship between the stress σ and the strain rate $\dot{\varepsilon}$ during hot deformation of the materials:

$$\sigma=K\dot{\varepsilon}^{m} \tag{22}$$

where K is the material coefficient and m is the strain rate sensitivity which is defined as

$$m=\frac{\mathrm{d}J}{\mathrm{d}G}=\frac{\dot{\varepsilon}\mathrm{d}\sigma}{\sigma\mathrm{d}\dot{\varepsilon}}=\frac{\dot{\varepsilon}\sigma\mathrm{d}\ln\sigma}{\sigma\dot{\varepsilon}\mathrm{d}\ln\dot{\varepsilon}}\approx\frac{\Delta\lg\sigma}{\Delta\lg\dot{\varepsilon}} \tag{23}$$

For the given strain ε and temperature T, the dissipated co-content J can be expressed as

$$J=\int_0^{\sigma}\dot{\varepsilon}\mathrm{d}\sigma=\frac{m\sigma\dot{\varepsilon}}{m+1} \tag{24}$$

It can be noted that only if m is a constant can Eq. (24) be satisfied. Generally, the value of m varies nonlinearly with the temperature T and the strain rate $\dot{\varepsilon}$. If m equals to 1, the material belongs to a perfect linear dissipation state, where the dissipated co-content J amounts to the maximum value $J_{\max}$ [17]:

$$J_{\max}=\frac{\sigma\dot{\varepsilon}}{2} \tag{25}$$

According to the combination of Eqs. (24) and (25), the efficiency of power dissipation is given by the dimensionless parameter η, which is expressed by

$$\eta=\frac{J}{J_{\max}}=\frac{2m}{m+1} \tag{26}$$

where η is a variable which is dependent on the temperature, the strain and the strain rate. At a given strain, the contour map of η with respect to the strain rate $\dot{\varepsilon}$ and the temperature T can be plotted so as to obtain the power dissipation map. In the map, each line represents a η value. A region with large η values is unable to stand for good workability since the η values may be very large in a region with bad workability. The inequation judging the processing stability of the metal, which is derived by ZIEGLER and YU [18], is described as

$$\frac{\mathrm{d}D}{\mathrm{d}R}>\frac{D}{R} \tag{27}$$

where $R=\sqrt{\dot{\boldsymbol{\varepsilon}}\cdot\dot{\boldsymbol{\varepsilon}}}$, D is the dissipation function at the specific temperature. According to DMM, D equals J. Therefore, for the uniaxial compression, Eq. (27) can be transformed into

$$\frac{\mathrm{d}J}{\mathrm{d}\dot{\varepsilon}}>\frac{J}{\dot{\varepsilon}} \tag{28}$$

which can be written as follows:

$$\frac{\mathrm{d}J}{\mathrm{d}\dot{\varepsilon}}=\frac{J\dot{\varepsilon}}{\dot{\varepsilon}J}\cdot\frac{\mathrm{d}J}{\mathrm{d}\dot{\varepsilon}}=\frac{J}{\dot{\varepsilon}}\cdot\frac{\mathrm{d}(\int(1/J)\mathrm{d}J)}{\mathrm{d}(\int(1/\dot{\varepsilon})\mathrm{d}\dot{\varepsilon})}=\frac{J}{\dot{\varepsilon}}\cdot\frac{\mathrm{d}\ln J}{\mathrm{d}\ln\dot{\varepsilon}} \tag{29}$$

Substituting the result of Eq. (29) into Eq. (28) gives

$$\frac{\mathrm{d}\ln J}{\mathrm{d}\ln\dot{\varepsilon}}>1 \tag{30}$$

Subsequently, substituting Eq. (24) into Eq. (30) results in

$$\frac{\mathrm{d}\ln J}{\mathrm{d}\ln\dot{\varepsilon}}=\frac{\mathrm{d}\ln(m/m+1)}{\mathrm{d}\ln\dot{\varepsilon}}+\frac{\mathrm{d}\ln\sigma}{\mathrm{d}\ln\dot{\varepsilon}}+\frac{\mathrm{d}\ln\dot{\varepsilon}}{\mathrm{d}\ln\dot{\varepsilon}}>1 \tag{31}$$

As a consequence, the expression for flow instability criterion is established as follows [19]:

$$\xi(\dot{\varepsilon})=\frac{\partial\ln\left(\frac{m}{m+1}\right)}{\partial\ln\dot{\varepsilon}}+m<0 \tag{32}$$

where $\xi(\dot{\varepsilon})$ can be regarded as a function of temperature and strain rate to obtain instability map. According to the instability map, metallurgical instability during plastic flow occurs in the region where $\xi(\dot{\varepsilon})$ is negative. The hot processing map is able to be obtained by combining the instability map with the power dissipation map.

3.3.2 Establishment and analysis of hot processing map

The curves of $\lg\sigma$ versus $\lg\dot{\varepsilon}$ are obtained according to the data illustrated in Fig. 2, as shown in Fig. 4. The curves are fitted by cubic spline and thus the values of m are determined on the basis of Eq. (23). Subsequently, the efficiencies of power dissipation η are calculated according to Eq. (26). As a result, the power dissipation maps illustrated in Fig. 5 are plotted by combining the values of η, T and $\lg\dot{\varepsilon}$.

By substituting the values of $\lg\dot{\varepsilon}$ and m into Eq. (32), the values of ξ at the corresponding temperatures and strain rates are calculated, and then the instability maps of equiatomic NiTi SMA are obtained by interpolation, as illustrated in Fig. 6. Consequently, the hot processing maps of the equiatomic NiTi SMA are established by combining the power dissipation maps with the instability maps, as shown in Fig. 7. It can be seen from Fig. 7 that the instability region is small and mainly corresponds to low temperatures as well as low strain rates when NiTi SMA is subjected to low strain. Furthermore, a very small instability region appears in

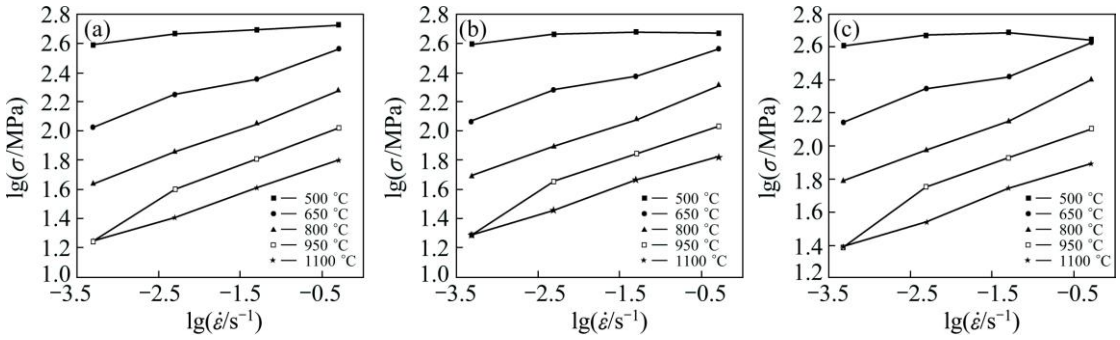

Fig. 4 Plots of $\lg\sigma$ vs $\lg\dot{\varepsilon}$ at various strains: (a) ε=0.4; (b) ε=0.8; (c) ε=1.2

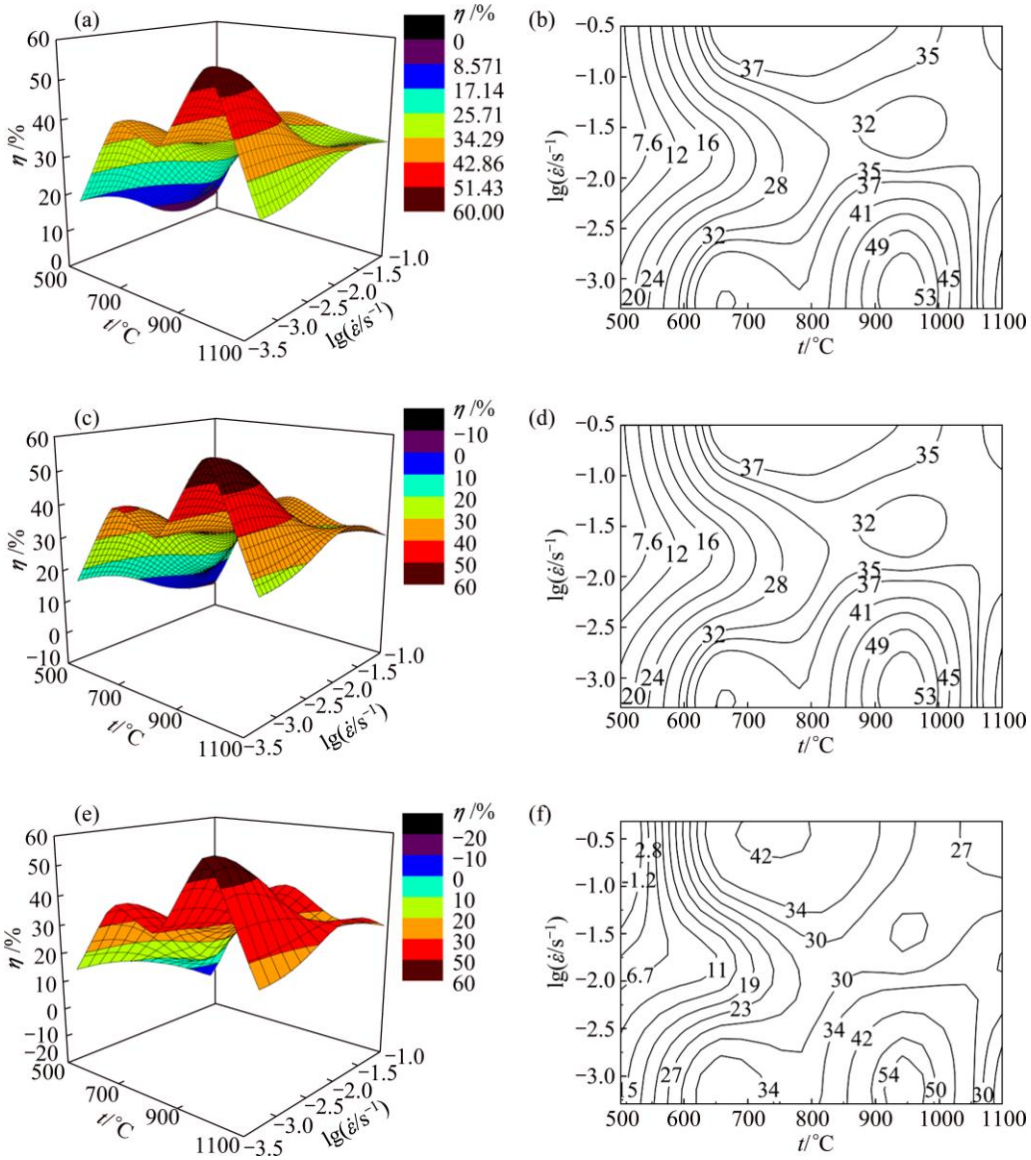

Fig. 5 3D (a, c, e) and 2D (b, d, f) power dissipation maps of equiatomic NiTi SMA at various strains: (a, b) ε=0.4; (c, d) ε=0.8; (e, f) ε=1.2

the case of medium strain rates in the temperature range of 900−1000 ℃. The area of instability regions increases with the increase of strain and covers the whole low-temperature region at the strain of 1.2. The instability region even appears at high temperatures and high strain rates when the true strain amounts to 1.2. Therefore, in the present study, it is preferable to process NiTi SMA at the temperatures ranging from 750 to 900 ℃.

The typical instability microstructures of equiatomic

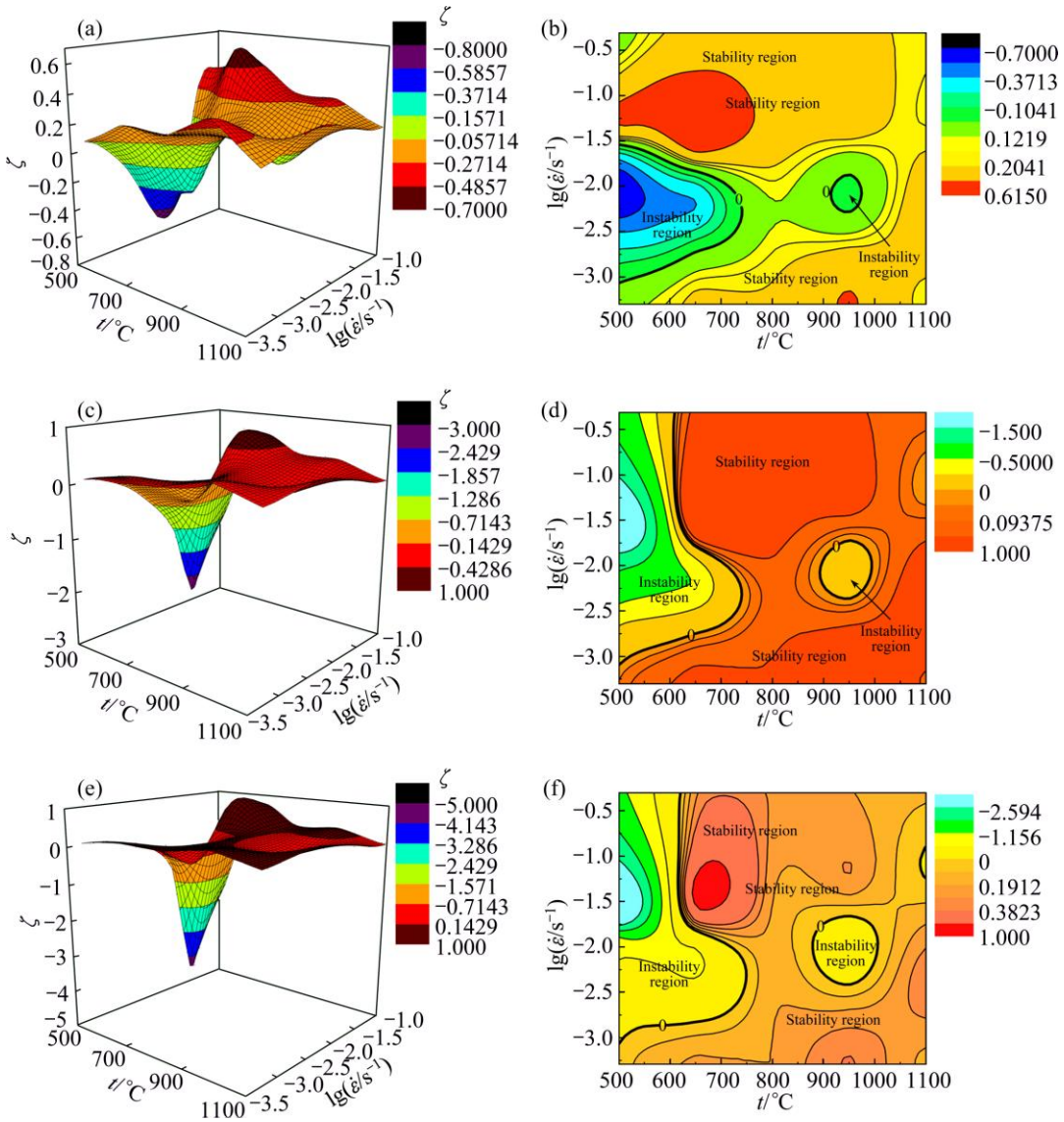

Fig. 6 3D (a, c, e) and 2D (b, d, f) instability maps of equiatomic NiTi SMA at various strains: (a, b) ε=0.4; (c, d) ε=0.8; (e, f) ε=1.2

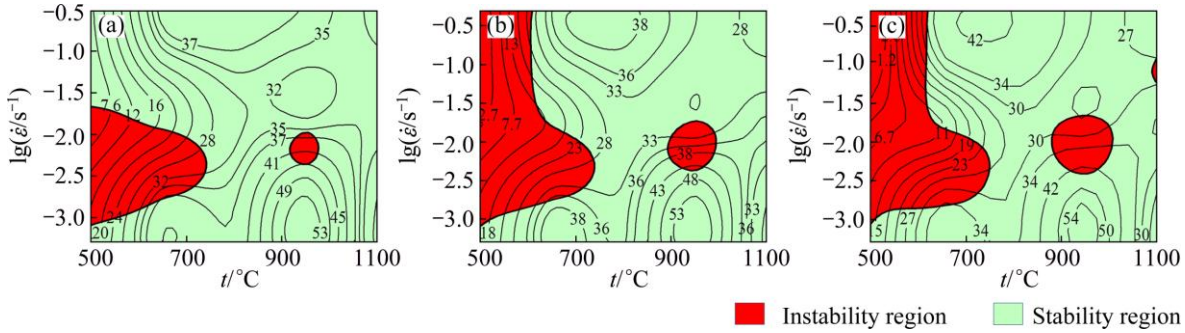

Fig. 7 Hot processing maps of equiatomic NiTi SMA at various strains: (a) ε=0.4; (b) ε=0.8; (c) ε=1.2

NiTi SMA at true strain of 1.2 are shown in Fig. 8, which gives the reasons why the instabilities occur at low temperatures and high temperatures. It can be found from Fig. 8(a) that the adiabatic shear bands, which are characterized by white and bright bands, appear at 500 ℃ and strain rate of 0.5 s^{-1}. The adiabatic shear bands are attributed to severe shear deformation in a local region, where a large amount of heat is generated and unable to dissipate, which consequently leads to more severe deformation. Another typical microstructure, which is obtained at 1100 ℃ and strain rate of 0.5 s^{-1}, is shown in Fig. 8(b). It can be seen that some grains

exhibit abnormal growth. The phenomenon results from the secondary recrystallization at high temperatures as well as high strain rates. The secondary recrystallization not only decreases the strength of the alloy, but also reduces its plasticity and toughness. Therefore, it is necessary to avoid processing equiatomic NiTi SMA in these instability regions.

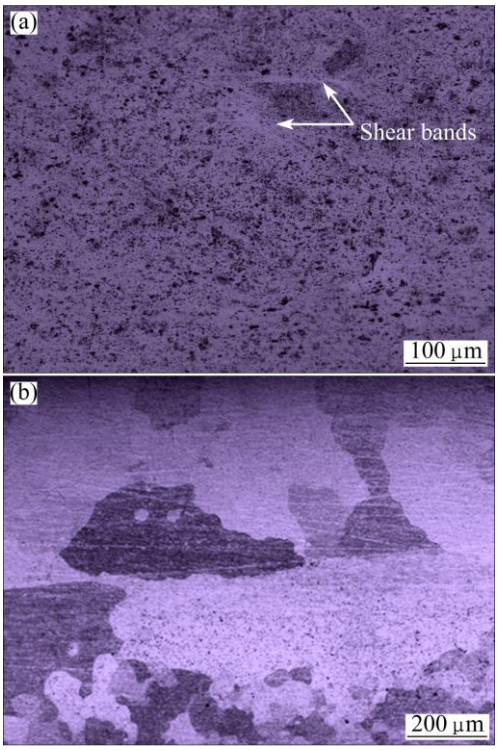

Fig. 8 Typical instability microstructures of equiatomic NiTi SMA at true strain of 1.2: (a) t=500 ℃, $\dot{\varepsilon}$=0.5 s^{-1}; (b) t=1100 ℃, $\dot{\varepsilon}$=0.5 s^{-1}

4 Conclusions

1) The flow stress of equiatomic NiTi SMA during isothermal deformation is significantly dependent on both the deformation temperature and the strain rate. The flow stress decreases with the increase of deformation temperature and the decrease of strain rate.

2) The constitutive equation of equiatomic NiTi SMA can be represented by Arrhenius-type equation, where the flow stress is a function of the deformation temperature and the strain rate. On the basis of compression test data, the constitutive equation of the alloy can be expressed as

$$\dot{\varepsilon}=5.3633\times10^{12}[\sinh(8.57\times10^{-3}\sigma)]^{3.9339}\times \exp\left(\frac{-3.0441\times10^{5}}{RT}\right).$$

3) The instability region of hot processing map increases with the increase of deformation extent. The instability occurs in the low and high temperature regions. Therefore, it is necessary to avoid processing equiatomic NiTi SMA in these regions. It is preferable to process NiTi SMA at the temperatures ranging from 750 to 900 ℃.

4) The instability region presents the adiabatic shear bands at low temperatures, but it exhibits the abnormal growth of the grains at high temperatures.

References

[1] PREDKI W, KNOPIK A, BAUER B. Engineering application of NiTi shape memory alloys [J]. Materials Science and Engineering A, 2008, 481−482: 598−601.

[2] JIANG Shu-yong, HU Li, ZHAO Ya-nan, ZHANG Yan-qiu, LIANG Yu-long. Plastic yielding of NiTi shape memory alloy under local canning compression [J]. Transactions of Nonferrous Metals Society of China, 2013, 23(10): 2905−2913.

[3] JIANG Shu-yong, TANG Ming, ZHAO Ya-nan, HU Li, ZHANG Yan-qiu, LIANG Yu-long. Crystallization of amorphous NiTi shape memory alloy fabricated by severe plastic deformation [J]. Transactions of Nonferrous Metals Society of China, 2014, 24(6): 1758−1765.

[4] JIANG Shu-yong, ZHANG Yan-qiu, ZHAO Ya-nan. Dynamic recovery and dynamic recrystallization of NiTi shape memory alloy under hot compression deformation [J]. Transactions of Nonferrous Metals Society of China, 2013, 23(1): 140−147.

[5] KIM K S, JEE K K, KIM W C, JANG W Y, HAN S H. Effect of heat treatment temperature on oxidation behavior in Ni−Ti alloy [J]. Materials Science and Engineering A, 2008, 481−482: 658−661.

[6] SADRNEZHAAD S K, MIRABOLGHASEMI S H. Optimum temperature for recovery and recrystallization of 52Ni48Ti shape memory alloy [J]. Materials and Design, 2007, 28(6): 1945−1948.

[7] JIANG Shu-yong, ZHAO Ya-nan, ZHANG Yan-qiu, TANG Ming, LI Chun-feng. Equal channel angular extrusion of NiTi shape memory alloy tube [J]. Transactions of Nonferrous Metals Society of China, 2013, 23(7): 2021−2028.

[8] LIN H C, WU S K. Effects of hot rolling on the martensitic transformation of an equiatomic Ti−Ni alloy [J]. Materials Science and Engineering A, 1992, 158(1): 87−91.

[9] JIANG Shu-yong, ZHANG Yan-qiu, ZHAO Ya-nan, TANG Ming, YI Wen-lin. Constitutive behavior of Ni−Ti shape memory alloy under hot compression [J]. Journal of Central South University, 2013, 20(1): 24−29.

[10] YEOM J T, JEOUNG H K, HONG J K, KIM S W, PARK C H, NAM T H, LEE K Y. Hot forging design of as-cast NiTi shape memory alloy [J]. Materials Research Bulletin, 2014, 58: 234−238.

[11] SHAMSOLHODAEI A, ZAREI-HANZAKI A, GHAMBARI M, MOEMENI S. The high temperature flow behavior modeling of NiTi shape memory alloy employing phenomenological and physical based constitutive models: A comparative study [J]. Intermetallics, 2014, 53: 140−149.

[12] MORAKABATI M, ABOUTALEBI M, KHEIRANDISH S, KARIMI TAHERI A, ABBASI S M. High temperature deformation and processing map of a NiTi intermetallic alloy [J]. Intermetallics, 2011, 19(10): 1399−1404.

[13] REZAEI ASHTIANI H R, PARSAB M H, BISADI H. Constitutive equations for elevated temperature flow behavior of commercial purity aluminum [J]. Materials Science and Engineering A, 2012, 545: 61−67.

[14] MANDAL S, RAKESH V, SIVAPRASAD P V, VENUGOPAL S, KASIVISWANATHAN K V. Constitutive equations to predict high

temperature flow stress in a Ti-modified austenitic stainless steel [J]. Materials Science and Engineering A, 2009, 500(1−2): 114−121.

[15] PRASAD Y V R K, SASIDHARA S, SIKKA V K. Characterization of mechanisms of hot deformation of as-cast nickel aluminide alloy [J]. Intermetallics, 2000, 8(9−11): 987−995.

[16] RAMANATHAN S, KARTHIKEYAN R, GUPTA M. Development of processing maps for Al/SiC_p composite using fuzzy logic [J]. Journal of Materials Processing Technology, 2007, 183(1): 104−110.

[17] ZENG W D, ZHOU Y G, ZHOU J, YU H Q, ZHANG X M, XU B. Recent development of processing map theory [J]. Rare Metal Materials and Engineering, 2006, 35(5): 673−677.

[18] ZIEGLER H, YU L K. Incompressible reiner-rivlin fluids obeying the orthogonality condition [J]. Ingenieur-Archiv, 1972, 41(2): 89−99.

[19] ŁUKASZEK-SOŁEK A, KRAWCZYK J. The analysis of the hot deformation behaviour of the Ti−3Al−8V−6Cr−4Zr−4Mo alloy, using processing maps, a map of microstructure and of hardness [J]. Materials and Design, 2015, 65: 165−173.

等原子比 NiTi 形状记忆合金高温塑性变形本构方程和热加工图

张艳秋[1]，江树勇[1]，赵亚楠[1]，刘思维[2]

1. 哈尔滨工程大学 机电工程学院，哈尔滨 150001；
2. 湖北省水利水电科学研究院，武汉 430070

摘 要：为了描述等原子比 NiTi 形状记忆合金在高温下的变形行为和热加工性能，通过在温度范围为 500~1100 ℃和应变速率范围为 0.0005~0.5 s^{-1} 的热压缩实验构建了该合金的 Arrhenius 型本构方程和热加工图。结果表明：热加工图的失稳区随着变形程度的增加而增大。失稳发生在低温区和高温区，低温区的失稳特征表现为绝热剪切带，而高温区的失稳特征则表现为晶粒的异常长大。因此，必须避免在这些失稳区域加工该等原子比 NiTi 形状记忆合金。加工该 NiTi 形状记忆合金的最佳温度范围为 750~900 ℃。

关键词：NiTi 合金；形状记忆合金；热塑性变形；本构方程；热加工图

(Edited by Mu-lan QIN)